Journal of Biomedical Optics

SPIEDigitalLibrary.org/jbo

Fluorescent probe for visualizing guanine-quadruplex DNA by fluorescence lifetime imaging microscopy

Ting-Yuan Tseng
Cheng-Hao Chien
Jen-Fei Chu
Wei-Chun Huang
Mei-Ying Lin
Cheng-Chung Chang
Ta-Chau Chang

SPIE

Fluorescent probe for visualizing guanine-quadruplex DNA by fluorescence lifetime imaging microscopy

Ting-Yuan Tseng,[a,b] Cheng-Hao Chien,[a,b] Jen-Fei Chu,[b] Wei-Chun Huang,[b,c,d] Mei-Ying Lin,[b] Cheng-Chung Chang,[e] and Ta-Chau Chang[a,b]
[a]National Yang-Ming University, Institute of Biophotonics, Taipei 11221, Taiwan
[b]Academia Sinica, Institute of Atomic and Molecular Sciences, Taipei 10617, Taiwan
[c]Academia Sinica, Taiwan International Graduate Program, Hsinchu 30013, Taiwan
[d]National Tsing-Hua University, Department of Chemistry, Hsinchu 30013, Taiwan
[e]National Chung-Hsing University, Graduate Institute of Biomedical Engineering, Taichung 402, Taiwan

Abstract. The importance of guanine-quadruplex (G4) is not only in protecting the ends of chromosomes for human telomeres but also in regulating gene expression for several gene promoters. However, the existence of G4 structures in living cells is still in debate. A fluorescent probe, 3,6-bis(1-methyl-2-vinylpyridinium) carbazole diiodide (*o*-BMVC), for differentiating G4 structures from duplexes is characterized. *o*-BMVC has a large contrast in fluorescence decay time, binding affinity, and fluorescent intensity between G4 structures and duplexes, which makes it a good candidate for probing G4 DNA structures. The fluorescence decay time of *o*-BMVC upon interaction with G4 structures of telomeric G-rich sequences is ~2.8 ns and that of interaction with the duplex structure of a calf thymus is ~1.2 ns. By analyzing its fluorescence decay time and histogram, we were able to detect one G4 out of 1000 duplexes *in vitro*. Furthermore, by using fluorescence lifetime imaging microscopy, we demonstrated an innovative methodology for visualizing the localization of G4 structures as well as mapping the localization of different G4 structures in living cells. [DOI: 10.1117/1.JBO.18.10.101309]

Keywords: fluorescent probe; DNA structure; G-quadruplex DNA; cell imaging; fluorescence lifetime; fluorescence lifetime imaging microscopy.

Paper 130115SSRR received Mar. 2, 2013; revised manuscript received Jun. 6, 2013; accepted for publication Jun. 7, 2013; published online Jul. 9, 2013.

1 Introduction

A large number of guanine-rich (G-rich) sequences are found in the human genome.[1–3] The G-rich sequences can easily form a G-quadruplex (G4) structure in the presence of salts *in vitro*.[4,5] It is suggested that the G4 structure is important not only in the human telomere for protecting the ends of chromosomes but also in the gene promoter for regulating gene expression. However, the challenging question is whether the G4 structure exists in living cells. Although some evidences of the presence of G4 structures *in vivo* have been reported in the ciliate *Stylonychia*,[6] the promoter of c-*myc*,[7] the human telomeres,[8] and the promoter of nonselenocysteine containing phospholipid hydroperoxide glutathione peroxidase (NPGPx),[9] the actual case in human cells is still in debate.[10]

It is known that the G-rich sequence can form various G4 structures and can possibly coexist in mixtures. For example, Hurley et al. reported that the sequence $d[(TG_4AG_3)_2TG_4AAG_2]$ (PU27) in c-*myc* gene promoter can form both intramolecular and intermolecular conformations in K^+ solution.[7] NMR and circular dichroism results showed that the monomeric parallel G4 structure is a major conformation for both PU27 and $d[TG(AG_3TG_4)_2AA]$ (PU22).[11] In addition, the broad envelope from the imino proton NMR spectra of the human telomeric sequence $d[AG_3(T_2AG_3)_3]$ (HT22) suggested the coexistence of two different G4 structures.[12,13] Moreover, telomere sequences with slight differences can adopt different types of G4 structures, such as a hybrid G4 structure of $d[TAG_3(T_2AG_3)_3]$ (HT23)[14] with three G-quartet layers versus a basket antiparallel G4 structure of $d[G_3(T_2AG_3)_3T]$ (HT21-T)[15] with two G-quartet layers in K^+ solution. At present, it is not clear which type of G4 structure is predominant in living cells if the G4 structure exists *in vivo*.

Fluorescence probes together with the advanced optical methods have presented many applications in biomedical sciences.[16–18] We have synthesized a fluorescent molecule, 3,6-bis (1-methyl-4-vinylpyridinium) carbazole diiodide (BMVC), to verify the presence of G4 structure in the human telomeres of metaphase chromosomes of nasopharyngeal carcinoma KJ-1 cells by using fluorescence lifetime imaging microscopy (FLIM).[19] Our finding was very recently confirmed by immunofluorescence for binder of G-quadruplex (BG4) on metaphase chromosomes isolated from Hela cancer cells.[20] They found that the majoriy (~75%) of BG4 foci were present outside the telomeres. In addition, the study on fixed cells also suggested that endogenous G4 structures are largely present outside the telomeres, implying that more G4 structures exist *in vivo*.

In order to map the localizations of endogenous G4 structures in living cells using a fluorescence probe such as BMVC, it must be able to discriminate the small amount of G4 structures from the large amount of duplexes in living cells. Since the two para-pyridinium groups in BMVC play a major binding role to the duplex DNA, we hypothesize that the change from para-pyridinium to ortho-pyridinium in BMVC could decrease the binding affinity to duplex DNA. Thus, a BMVC isomer, *o*-BMVC, was synthesized and compared to BMVC. Previously, we shown that both BMVC and *o*-BMVC are good G4 stabilizers.[21] In this work, we demonstrate that *o*-BMVC is indeed a better G4

Address all correspondence to: Ta-Chau Chang, Institute of Atomic and Molecular Sciences, Academia Sinica, P.O. Box 23-166, Taipei 106, Taiwan. Tel: +886-2-23668231; E-mail: tcchang@po.iams.sinica.edu.tw

fluorescent probe with a much higher binding preference to HT24 than linear duplex $[d(GCGCAATTGCGC)]_2$ (LD12) compared to that of BMVC. Moreover, the fluorescence decay time of *o*-BMVC is longer than that of BMVC upon interaction with G4 structure, and much longer than that of LD12 or calf thymus interacting with either *o*-BMVC or BMVC. Thus, it gives a wider window with better time-resolution in FLIM imaging and is furthermore used to differentiate G4 structure from duplex structure in living cells. Table 1 lists the DNA sequences studied in this work.

2 Materials and Methods

2.1 *Chemicals*

The synthesis of *o*-BMVC is briefly described in Fig. 1. 3,6-Dibromocarbazole (10 mmole, Aldrich, St. Louis, MO) was added into a high-pressure bottle containing the mixture of palladium(II) acetate (25 mg, Strem, Newburyport, MA) and tri-*o*-tolyl phosphine (250 mg, Aldrich). To this, the solvent pair (tri-ethylamine 15 ml/acetonitrile 45 ml) and 2-vinylpyridine (30 mmole, Merck, Darmstadt, Germany) were added. The bottle was sealed after bubbling 10 min with nitrogen. After keeping the system under ~105°C for two days, the precipitant was collected and then extracted with H_2O/CH_2Cl_2 twice. The insoluble solids in the CH_2Cl_2 layer were filtered, collected, and washed with hot tetrahydrofuran (THF); then the filtrates were dried by $MgSO_4$. Crude powder was purified by flash column chromatography with acetone/n-hexane as eluent gradient to collect the yellow powder, precursor of *o*-BMVC (compound 2, shown in Fig. 1). Yield: 72%, melting point (mp): 254 to 256°C, molecular weight (Mw): 373. ^{1}H NMR [dimethyl sulfoxide (DMSO-d6)]: δ(ppm) = 11.5 (s, 1H, NH), 8.57 (dd, J = 5.7, 1.38 Hz, 2H), 8.48 (s, 2H), 7.85 (d, J = 16.2 Hz, 2H), 7.78 (m, 2H), 7.74 (dd, J = 9.0, 1.26 Hz, 2H), 7.55 (d, J = 7.5 Hz, 2H), 7.50 (d, J = 7.2 Hz, 2H), 7.31 (d, J = 16.2 Hz, 2H), 7.23 (dd, J = 7.5, 6.4 Hz, 2H). After refluxing compound 2 with excess CH_3I in THF/dimethylformamide (DMF) (2 : 1) for 4 h, the orange powder, *o*-BMVC, was collected with a hot filter (Yield: 95%, mp >300°C, Mw: 657). Data for *o*-BMVC: ^{1}H NMR (DMSO-d6): δ(ppm) = 11.97 (s, 1H, NH), 8.87 (dd, J = 6.3, 1.2 Hz, 2H), 8.84 (s, 2H), 8.47 (d, J = 8.7 Hz, 2H), 4,42 (s, 6H), ESI/MS (m/z: $[M+H]^+$ 201.68 (exclude I^-), element analysis (657 + 1.5 H_2O): calc (obs%) C: 49.12 (49.17), H: 4.09 (4.03), N: 6.14 (6.12).

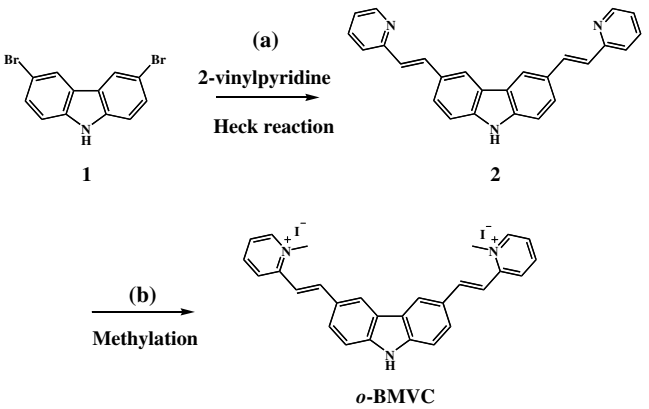

Fig. 1 The brief scheme of *o*-BMVC synthesis.

Table 1 DNA sequences studied in this work and fluorescence decay times of BMVC and *o*-BMVC upon interaction with these DNA sequences.

Sequence	DNA name	BMVC (ns)	*o*-BMVC (ns)
$TAG_3(T_2AG_3)_3$	HT23	~2.3	~2.8
$(T_2AG_3)_4$	HT24	~2.0	~2.6
$TAG_3(T_2AG_3)_3TT$	HT25	~2.0	~2.6
$(G_3T_2A)_3G_3T$	HT21-T	~1.7	~2.4
$G_2T_2G_2TGTG_2T_2G_2$	TBA	~2.3	~4.0
$TGAG_3TG_4AG_3TG_4AA$	PU22	~2.0	~3.0
$(TAG_3)_2TG_3TAG_3$	GT19	~2.1	~3.0
$G_3(TG_3)_3$	T3	~2.0	~3.0
$(G_3C)_4$	T40214	~2.0	~3.0
$GCGCA_2T_2GCGC$	LD12	~1.3	~1.0
DNA from calf thymus	Calf thymus	~1.7	~1.2

2.2 *DNA Samples*

All oligonucleotides were purchased from Biobasic Inc., Markham, Ontario, Canada. A buffer solution (pH 7.5) that consisted of 10 mM Tris-HCl and 150 mM KCl was used for all experiments. Buffer solutions mixed with oligonucleotides were heated to 95°C for 5 min and cooled slowly at 1°C/min to room temperature followed by storage at 4°C over night before use.

2.3 *Cell Cultures*

CL1-0 human lung cancer cell line was kindly provided by Prof. C. T. Chen of National Taiwan University and grown in RPMI1640 supplemented with 10% fetal bovine serum.

2.4 *Absorption and Fluorescence Spectra*

Absorption spectra were taken on a UV-visible spectrophotometer (HELIOS α, Thermo Fisher Scientific, USA), and fluorescence spectra were recorded on a spectrofluorometer (LS-55, PerkinElmer, USA) with a 2-nm bandpass in a 1-cm cell length at room temperature.

2.5 *Fluorescence Lifetime Imaging Microscopy*

The setup of FLIM consists of a picosecond diode laser emitting at 470 nm (LDH470, PicoQuant, Germany) with ~70 ps pulse width to excite *o*-BMVC under a scanning microscope (IX-71 and FV-300, Olympus, Japan). The fluorescence of *o*-BMVC was collected by a 60× NA = 1.42 oil-immersion objective (PlanApoN, Olympus, Japan), passing through a 550/80 bandpass filter (Chorma, USA), and then detected by a fast photomultiplier tube (PMA182, PicoQuant). The fluorescence lifetime was analyzed by using a time-correlated single photon counting (TCSPC) module and software (TimeHarp-200 and

SymPhoTime, PicoQuant). The FLIM image was constructed from pixel-by-pixel lifetime information.

2.6 *Confocal Microscopy*

CL1-0 cells were incubated with 5 μM *o*-BMVC for 2 h and were subsequently treated with 40 nM MitoTracker red CMXRos (Invitrogen, Carlsbad, CA) for 30 min. Stained cells were washed twice with phosphate-buffered saline and visualized by confocal microscopy. Fluorescence excitation/emission was carried out at 458/500 to 600 nm for *o*-BMVC channel and at 532/600 to 700 nm for MitoTracker red channel.

3 Results and Discussion

3.1 *Absorption and Fluorescence Spectra*

Figure 2 shows the absorption and fluorescence spectra of free *o*-BMVC and its complex with a number of G4 DNA of HT23, HT21-T, TBA, PU22, GT19, and two duplex DNA, LD12 and calf thymus, in 150 mM K^+ solution. The absorption maximum of *o*-BMVC at ~420 nm is red-shifted to ~435 nm upon interaction with LD12 and calf thymus, and further red-shifted to ~460 nm in the presence of G4 structures. In addition, the molar absorption coefficient is decreased by 10 to 15% for duplexes and decreased even more for G4 structures. The fluorescence peak of *o*-BMVC shows a slight difference upon interaction with G4 structures at ~555 nm and with duplexes at ~545 nm. Moreover, Fig. 2 shows that the fluorescence of *o*-BMVC increases 80 to 120 times in the presence of these G4 structures and ~20 times in the presence of these duplexes. The fluorescence enhancement ratio upon *o*-BMVC binding to quadruplex and duplex DNA is estimated to be ~5:1. In comparison, the enhancement of BMVC fluorescence is slightly lower upon interaction with HT24 (quadruplex) than that of LD12 (duplex) in our previous work.[22]

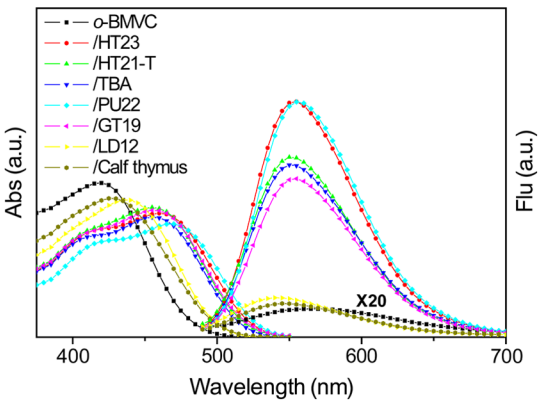

Fig. 2 The absorption and fluorescence spectra of *o*-BMVC molecule and its mixture with HT23, HT21-T, TBA, PU22, GT19, LD12, and calf thymus, in 150 mM K^+ solution. Molar concentration *o*-BMVC: DNA = 1:3.

Fluorescence titration was carried out to measure the binding affinities of *o*-BMVC to LD12 and HT24. Figure 3 shows the fluorescence spectra of 10 μm of *o*-BMVC by adding DNA from 0.25 to 8 μm. The fluorescence intensity used to construct the binding plots of γ versus C_f is shown in the inset. The binding ratio γ is defined as C_b/C_{DNA}, where C_f, C_b, and C_{DNA} are the molar concentrations of free ligand, bound ligand, and DNA, respectively. The difference between C_t and C_b gives the magnitude of C_f, where C_t is the total concentration of ligand. Binding parameters can be obtained by fitting the plots with a multiple-equivalent-site model.[23]

$$\gamma = n\mathrm{K}C_f/(1+\mathrm{K}C_f),$$

where K is the equilibrium binding constant and n represents the average number of ligands bound per each DNA structure. Note that this equation is identical to the Scatchard equation, $\gamma/C_f = \mathrm{K}(n-\gamma)$. Using the binding plots of γ versus C_f, the problem of obtaining K and n values from slightly nonlinear Scatchard plots becomes irrelevant.[24] Here, the calculated binding parameters are $\mathrm{K} \sim 3.43 \times 10^5$ with $n \sim 5.5$ for LD12 and $\mathrm{K} \sim 3.0 \times 10^7$ with $n \sim 3.2$ for HT24, indicating that the binding affinity of *o*-BMVC to HT24 G4 DNA is much better than that to LD12 duplex DNA. The binding preference of *o*-BMVC to G4 structures over duplexes is improved by almost an order of magnitude over that of BMVC. This difference is likely due to the structural difference between these two isomers, i.e., the ortho form for *o*-BMVC forces the two positive charges toward outside, while the para form for BMVC shows less interference between the two positive charges. The two positive charges on the tip of the crescent-shaped BMVC can easily interact with the minor groove of LD12,[25] while there is no such binding mode for *o*-BMVC to LD12. It is rational that the binding affinity of BMVC to LD12 is approximately one order of magnitude higher than *o*-BMVC to LD12.

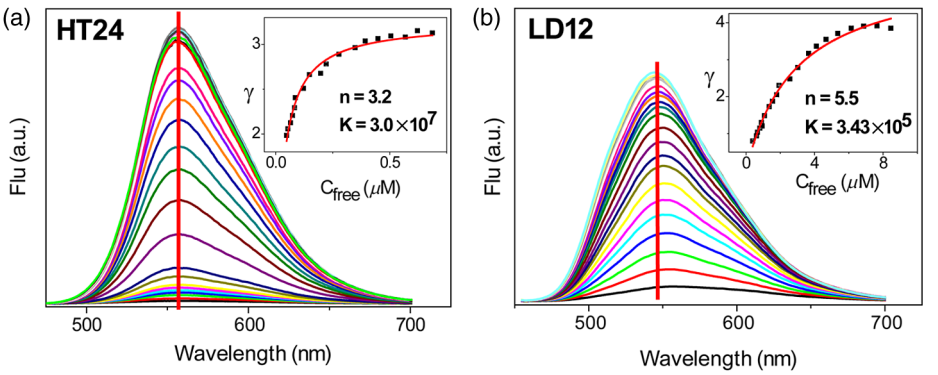

Fig. 3 Fluorescence titration of 10 μM *o*-BMVC by adding HT24 (a) and LD12 (b) from 0.25 to 8 μM in 150 mM K^+ solution. The inset shows the binding plots of γ versus C_f for the titration.

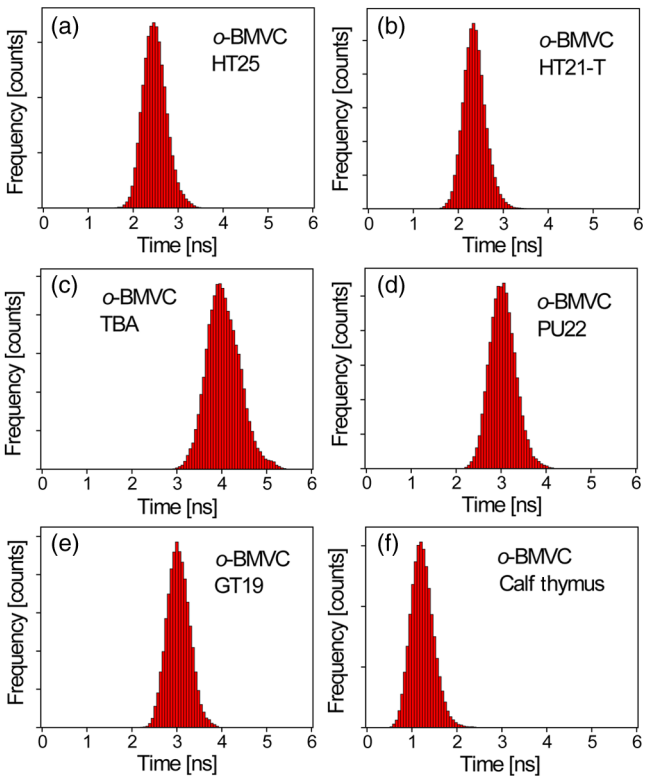

Fig. 4 The histograms of the fluorescence decay time of *o*-BMVC upon interaction with HT25 (a), HT21-T (b), TBA (c), PU22 (d), GT19 (e), and calf thymus (f) in 150 mM K^+ solution. Molar concentration *o*-BMVC:DNA = 1:3.

3.2 *Fluorescence Decay of o-BMVC upon Interaction with Various DNA Structures*

o-BMVC is a molecular rotor, where the intramolecular twist of the vinyl group in bridging the carbazole and pyridinium cation of *o*-BMVC plays a major role in determining its fluorescence behavior. Since different DNA structures may have different binding sites to *o*-BMVC, it is possible to distinguish different DNA structures by monitoring their fluorescence decay times. Thus, we have used FLIM to measure the fluorescence decay time of *o*-BMVC upon interaction with these DNA. The sample was prepared on a cover-slip, and the decay signal was measured by using TCSPC equipped with a 70-ps laser pulse at 470 nm. Figure 4 shows the histograms of the fluorescence decay time of *o*-BMVC upon interaction with HT25, HT21-T, TBA, PU22, GT19, and calf thymus in 150 mM K^+ solution. The peak center of the *o*-BMVC decay time is measured to be ~2.6 ns for HT25, ~2.4 ns for HT21-T, ~4.0 ns for TBA, ~3.0 ns for PU22, ~3.0 ns for GT19, and ~1.2 ns for calf thymus. In addition, the ~3.0 ns decay time is also measured upon interaction with T3 and T40214 (data not shown), whereas PU22, GT19,[26] T3,[27] and T40214[28] are all predominated by the parallel-type G4 structure. This is probably due to the same end-quartet binding site without the loop base that they have for *o*-BMVC.[29] For comparison, Table 1 lists fluorescence decay times of both BMVC and *o*-BMVC upon interaction with these DNA sequences. The key finding is that the fluorescence decay time of *o*-BMVC is longer than that of BMVC upon interaction with G4 structures, while the fluorescence decay time of *o*-BMVC is slightly shorter than that of BMVC upon interaction with duplexes. The decay time difference between quadruplex and duplex DNA is much larger for *o*-BMVC than for BMVC, which is pivotal to the study of cellular imaging, i.e., 2.8 ns in the presence of HT23 and 1.2 ns in the presence of calf thymus for *o*-BMVC versus 2.3 ns in the presence of HT23 and 1.7 ns in the presence of calf thymus for BMVC.

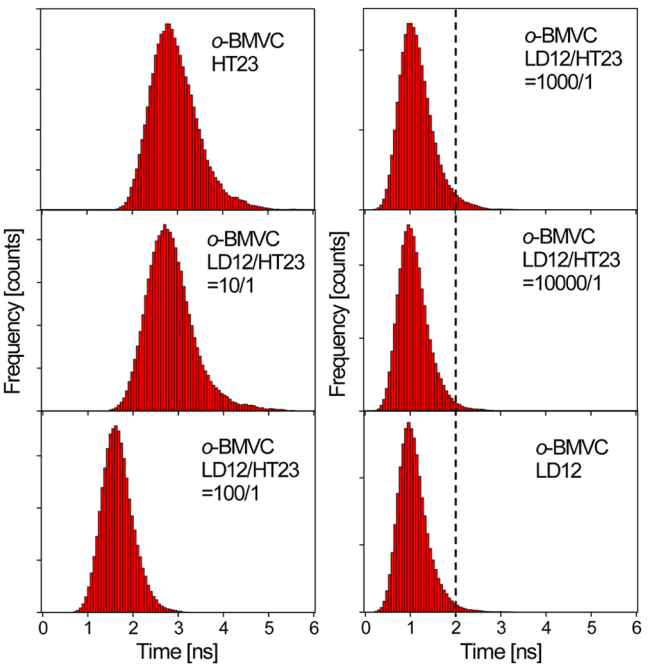

Fig. 5 The histograms of the fluorescence decay time of *o*-BMVC upon interaction with the mixtures of LD12 and HT23 at 1:0, 10:1, 100:1, 1000:1, 10,000:1, and 0:1 molar ratio in 150 mM K^+ solution.

In our previous work, we had used BMVC to verify the presence of G4 structure in the human telomeres of metaphase chromosomes.[19] Here *o*-BMVC is a better fluorescence probe for differentiating the G4 structures from duplexes than BMVC because *o*-BMVC has a large contrast of decay time, binding affinity, and fluorescent intensity between the G4 structures and the duplexes. To further test the detecting limit of the G4 structure revealed by *o*-BMVC, we have conducted competition analysis by mixing 30 μM of LD12 with various concentrations of HT23 using FLIM. Figure 5 shows the histograms of the fluorescence decay time of *o*-BMVC upon interaction with the mixture of LD12 and HT23 at 0:1, 10:1, 100:1, 1000:1, 10,000:1, and 1:0 molar ratios. Our results suggest that *o*-BMVC is able to detect one HT23 out of 1000 LD12 and possibly one HT23 out of 10,000 LD12.

3.3 *Fluorescent Bioimaging of o-BMVC in CL1-0 Cancer Cells*

We now use *o*-BMVC as a turn-on probe to image the possible G4 structure in human CL1-0 lung cancer cells. Our FLIM images show that *o*-BMVC is mainly distributed in the cytoplasm of CL1-0 living cells and found less in the nucleus. In contrast, BMVC is mainly located in the nucleus and found less in the cytoplasm. To determine the intracellular localization of *o*-BMVC, Fig. 6 shows confocal images of CL1-0 cells incubated with *o*-BMVC for 2 h and then stained by MitoTracker red. *o*-BMVC fluorescence overlaps well with MitoTracker red (83.1 ± 9.9%), implying that *o*-BMVC mainly localizes in the mitochondria of the CL1-0 cancer cells. Different cellular

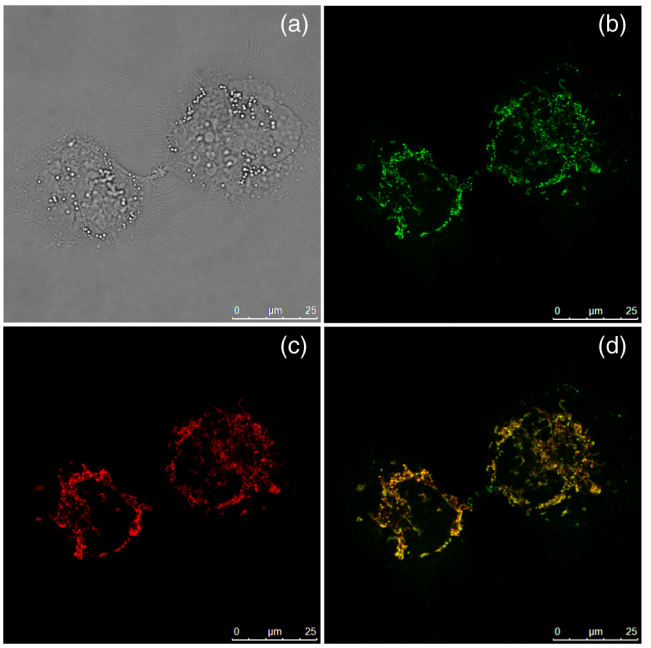

Fig. 6 CL1-0 cancer cells incubated with *o*-BMVC for 2 h and then stained by MitoTracker red, shown as the bright field image (a), confocal images at *o*-BMVC channel (green) (b) and at MitoTracker channel (red) (c), and their merged image (d).

localizations of BMVC and *o*-BMVC are probably due to different lipophilicities. BMVC with low lipophilicity (log P ~ −1.97) localized primarily to the nucleus, while *o*-BMVC with higher lipophilicity (log P ~ −1.4) localized primarily to the mitochondria.

Considering the large difference between the decay times of *o*-BMVC upon interaction with G4 structures and duplexes (Fig. 4), we further used FLIM for visualizing the possible G4 structures in living cells. Figure 7(a) and 7(d) shows the FLIM images of living CL1-0 cells incubated with *o*-BMVC and BMVC, respectively. For *o*-BMVC, the image shows strong fluorescence in the cytoplasm and weak fluorescence in the nucleus of the cell. According to Table 1, we assume the decay time region of 2.4 to 2.8 ns is mainly due to telomeric G4 structures, while the region longer than 2.8 ns is mainly due to parallel-type G4 structures and other specific G4 structures. For clarity, we set a certain decay time (2.4 or 2.8 ns) and use only white and red pseudocolors to present these figures, where the white color stands for decay times longer than that time (designated as mode 1) and the red color stands for shorter decay times (designated as mode 2), as shown in Fig. 7(b), 7(c), 7(e), and 7(f). Interestingly, in Fig. 7(b), we found mode 1 (white) spots in both the nucleus and cytoplasm of the cell. Although only a small amount of *o*-BMVC can enter the nucleus, this may be desirable since the much higher binding affinity of *o*-BMVC to the G4 structures over the duplexes (~100:1) allows this small amount of *o*-BMVC to target G4 structures in the nucleus. As a result, this will avoid the ensemble average effect from the interaction of *o*-BMVC with the large amount of duplex DNA structures in the nucleus. The large decay time contrast of *o*-BMVC upon interaction between quadruplex and duplex DNA is sufficient to differentiate the possible G4 structures located in the nucleus. On the other hand, since in the cytoplasm *o*-BMVC mainly localizes in mitochondria, the observation of mode 1 in the cytoplasm may be mainly due to possible G4 structures in mitochondrial DNA, in which there are many repeats of G-rich motifs (NCBI Reference Sequence: NC 001807.4).

We further observe that there are fewer mode 1 spots at 2.8 ns time mode, and these spots almost totally disappear at 3.2 ns time mode (data not shown). Here we assume that those mode 1 spots that appeared at 2.4 ns time mode, but disappeared at 2.8 ns, are probably not due to parallel-type G4 structures. Considering the fluorescence decay time of *o*-BMVC is ~3.0 ns upon interaction with the parallel G4 structures, including PU22, GT19, T3, and T40214 measured in this work, it is likely that the nonparallel G4 structure is predominant in living cells. The much lower signal (mode 1 spots) of CL1-0 cells incubated with BMVC at 2.4 and 2.8 ns, shown in Fig. 7(e) and 7(f), further confirms that the longer decay time of *o*-BMVC to G4

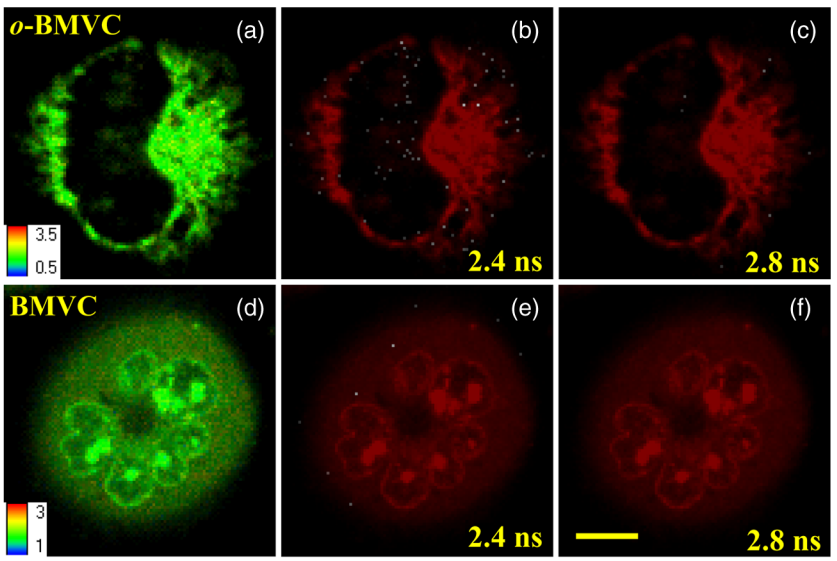

Fig. 7 FLIM images of living CL1-0 cells incubated with *o*-BMVC [(a), (b), (c)] or BMVC [(d), (e), (f)] for 2 h. (b) and (e) are presented in pseudocolors of white (decay time >2.4 ns) and red (decay time <2.4 ns). (c) and (f) are presented in pseudocolors of white (decay time >2.8 ns) and red (decay time <2.8 ns). Scale bar: 10 μm.

structures is critical for depicting the existence of G4 structures in living cells. These data provide "proof-of-concept" evidence for using *o*-BMVC as a sensitive and specific fluorescent probe for visualizing the possible G4 structures.

4 Conclusion

In summary, we have illustrated that an *o*-BMVC molecule is a better fluorescent probe for more specific binding to G4 DNA than BMVC. The binding preference to G4 structures over duplexes is improved by almost an order of magnitude. In addition, the longer decay time of *o*-BMVC upon interaction with G4 structures of telomeric G-rich sequences (~2.8 ns) than with duplex structure of calf thymus (~1.2 ns) is sufficient to differentiate these structures by using discrete time mode in FLIM images. Considering that there are many potential G4 forming sequences in the human genome, the interaction of *o*-BMVC with some of them may have even longer decay times, such as the ~4.0 ns upon interaction with TBA. These longer decay times are even better for the verification of the presence of G4 structures in living cells. At present, FLIM of CL1-0 cells stained by *o*-BMVC allows us to visualize the location characterized by the long decay time in living cells. We consider that these locations with the longer decay time are likely due to the presence of G4 structures. The potential application of *o*-BMVC to map the localizations of various G4 structures deserves further investigation.

Acknowledgments

This work was supported by Academia Sinica (AS-102-TP-A07) and the National Science Council of the Republic of China (Grant NSC-101-2113-M-001-022). We thank Professor Fu-Jen Kao at National Yang-Ming University for his expert guidance on the construction of fluorescence lifetime imaging microscopy. We thank Dr. Margaret Hsin-Jui Kuo (Academia Sinica) for her invaluable discussion.

References

1. A. K. Todd, M. Johnston, and S. Neidle, "Highly prevalent putative quadruplex sequence motifs in human DNA," *Nucleic Acids Res.* **33**(9), 2901–2907 (2005).
2. J. L. Huppert and S. Balasubramanian, "Prevalence of quadruplexes in the human genome," *Nucleic Acids Res.* **33**(9), 2908–2916 (2005).
3. J. Eddy and N. Maizels, "Gene function correlates with potential for G4 DNA formation in the human genome," *Nucleic Acids Res.* **34**(14), 3887–3896 (2006).
4. M. Gellert, M. N. Lipsett, and D. R. Davies, "Helix formation by guanylic acid," *Proc. Nat. Acad. Sci.* **48**(12), 2013–2018 (1962).
5. D. Sen and W. Gilbert, "Formation of parallel four-stranded complexes by guanine-rich motifs in DNA and its implications for meiosis," *Nature* **334**(6180), 364–366 (1988).
6. H. J. Lipps and D. Rhodes, "G-quadruplex structure: in vivo evidence and function," *Trends Cell Biol.* **19**(8), 414–422 (2009).
7. A. Siddiqui-Jain et al., "Direct evidence for a G-quadruplex in a promoter region and its targeting with a small molecule to repress c-MYC transcription," *Proc. Nat. Acad. Sci. U. S. A.* **99**(18), 11593–11598 (2002).
8. C. C. Chang et al., "Detection of quadruplex DNA structures in human telomeres by a fluorescent carbazole derivative," *Anal. Chem.* **76**(15), 4490–4494 (2004).
9. P. C. Wei et al., "A *cis*-element with mixed G-quadruplex structure of NPGPx promoter is essential for nucleolin-mediated transactivation on non-targeting siRNA stress," *Nucleic Acids Res.* **41**(3), 1533–1543 (2013).
10. C. Schaffitzel et al., "In vitro generated antibodies specific for telomeric guanine-quadruplex DNA react with *Stylonychia lemnae macronuclei*," *Proc. Natl. Acad. Sci. U. S. A.* **98**(15), 8572–8577 (2001).
11. A. T. Phan, Y. S. Modi, and D. J. Patel, "Propeller-type parallel-stranded G-quadruplexes in the human c-myc promoter," *J. Am. Chem. Soc.* **126**(28), 8710–8716 (2004).
12. J. Li et al., "Not so crystal clear: the structure of the human telomere G-quadruplex in solution differs from that present in a crystal," *Nucleic Acids Res.* **33**(14), 4649–4659 (2005).
13. A. Ambrus et al., "Human telomeric sequence forms a hybrid-type intramolecular G-quadruplex structure with mixed parallel/antiparallel strands in potassium solution," *Nucleic Acids Res.* **34**(9), 2723–2735 (2006).
14. K. N. Luu et al., "Structure of the human telomere in K+ solution: an intramolecular (3 + 1) G-quadruplex scaffold," *J. Am. Chem. Soc.* **128**(30), 9963–9970 (2006).
15. K. W. Lim et al., "Structure of the human telomere in K+ solution: a stable basket-type G-quadruplex with only two G-tetrad layers," *J. Am. Chem. Soc.* **131**(12), 4301–4309 (2009).
16. E. S. Yeung, "Dynamics of single biomolecules in free solution," *Annual Rev. Phys. Chem.* **55**, 97–126 (2004).
17. J. R. Unruh et al., "Orientational dynamics and dye-DNA interactions in a dye-labeled DNA aptamer," *Biophys. J.* **88**(5), 3455–3465 (2005).
18. P. S. Shirude et al., "Single-molecule conformational analysis of G-quadruplex formation in the promoter DNA duplex of the proto-oncogene c-kit," *J. Am. Chem. Soc.* **129**(24), 7484–7485 (2007).
19. C. C. Chang et al., "Verification of antiparallel G-quadruplex structure in human telomeres by using two-photon excitation fluorescence lifetime imaging microscopy of the 3,6-bis(1-methyl-4-vinylpyridinium) carbazole diiodide molecule," *Anal. Chem.* **78**(8), 2810–2815 (2006).
20. G. Biffi et al., "Quantitative visualization of DNA G-quadruplex structures in human cells," *Nat. Chem.* **5**(3), 182–186 (2013).
21. J. F. Chu et al., "A novel method for screening G-quadruplex stabilizers to human telomeres," *J. Chin. Chem. Soc.* **58**(3), 296–300 (2011).
22. C. C. Chang et al., "A fluorescent carbazole derivative: high sensitivity for quadruplex DNA," *Anal. Chem.* **75**(22), 6177–6183 (2003).
23. J. B. Chaires, "Analysis and interpretation of ligand-DNA binding isotherms," *Methods Enzymol.* **340**, 3–22 (2001).
24. C. C. Chang et al., "Investigation of spectral conversion of d(TTAGGG)4 and d(TTAGGG)13 upon potassium titration by a G-quadruplex recognizer BMVC molecule," *Nucleic Acids Res.* **35**(9), 2846–2860 (2007).
25. F. A. Tanious et al., "Effects of compound structure on carbazole dication-DNA complexes: tests of the minor-groove complex models," *Biochemistry* **39**(39), 12091–12101 (2000).
26. L. Hu et al., "Giardia telomeric sequence d(TAGGG)4 forms two intramolecular G-quadruplexes in K+ solution: effect of loop length and sequence on the folding topology," *J. Am. Chem. Soc.* **131**(46), 16824–16831 (2009).
27. V. Viglasky, L. Bauer, and K. Tluckova, "Structural features of intra- and intermolecular G-quadruplexes derived from telomeric repeats," *Biochemistry* **49**(10), 2110–2120 (2010).
28. N. Q. Do et al., "Stacking of G-quadruplexes: NMR structure of a G-rich oligonucleotide with potential anti-HIV and anticancer activity," *Nucleic Acids Res.* **39**(21), 9448–9457 (2011).
29. D. Y. Yang, T. C. Chang, and S. Y. Sheu, "Interaction between human telomere and a carbazole derivative: a molecular dynamics simulation of a quadruplex stabilizer and telomerase inhibitor," *J. Phys. Chem. A* **111**(38), 9224–9232 (2007).